A&A 424, 415–428 (2004)
DOI: 10.1051/0004-6361:20034107
© ESO 2004

Astronomy & Astrophysics

# Dark energy versus $\Omega_m = 1$ in the growth of matter perturbations

M. Membrado[1] and J. A. L. Aguerri[2]

[1] Departamento de Física Teórica, Universidad de Zaragoza, 50009 Zaragoza, Spain
e-mail: membrado@unizar.es
[2] Instituto de Astrofísica de Canarias, 38200 La Laguna, Spain
e-mail: jalfonso@ll.iac.es

Received 24 July 2003 / Accepted 2 June 2004

**Abstract.** We explore the possibility of discriminating dark energy models from the study of the growth of matter perturbations. For the sake of simplicity, instead of dealing with a great number of models, we have chosen a simple model of dark energy ($p_x = \omega_0 \rho_x^\gamma$, with $\omega_0 < 0$ and $\gamma > 0$; $p_x$, and $\rho_x$ being pressure and energy density), which is able to reproduce a great number of different behaviours. A combination of WMAP data with other results have been used to estimate model parameters. The study has been made for collapsing shells in spherical clusters virialized at redshifts $z = 1$, 0.1 and 0.025 with line-of-sight velocity dispersion $\sigma_{los} = 750$ and 1000 km s$^{-1}$. According to shell velocities, our dark energy models are clearly differentiated from the $\Omega_{m0} = 1$ model (the greater the $\sigma_{los}$ is, the more differentiated the models are). However, the differences among dark energy models are not so large. From our results, the nearest clusters with large $\sigma_{los}$ are the idoneous ones to discriminate models. In fact, we think that from observations of caustics in nearby spherical clusters, it would be possible to make an estimation of $\Omega_{m0}$.

**Key words.** cosmology: theory

## 1. Introduction

It is well known that if our Universe, which seems to be flat (Efstathiou et al. 1998), contained just radiation and matter, it would be too youthful with respect to determinations of the ages of the oldest stars (Chaboyer et al. 1995). This fact made to think in the presence of another component in the Universe. Thus, it is assumed that, in addition to ordinary Cold Dark Matter (CDM), there is a component, named $x$-matter or "dark energy", whose pressure, $p_x$, is a negative function of the density, $\rho_x$. This new component, not only solves the flatness dilemma, but also other cosmological problems such as the strong evidence that the expansion of the Universe is speeding up, rather than slowing down (see, for example: Perlmutter et al. 1997, 1999; Schmidt et al. 1998).

The first models for dark energy were hydrodynamical models, but quickly, dynamical scalar field models were proposed. The first hydrodynamical models were developed by Steinhardt (1996), and Turner & White (1997), which proposed $\omega$-constant models ($p_x = \omega_0 \rho_x$, with $-1 < \omega_0 < 0$). Examples of these models are the cosmological constants ($\rho_x = $ const.; $\omega_0 = -1$) and the frustrated networks of topological defects (Vilenkin 1984; Spergel & Pen 1997), such as strings or walls ($\omega_0 = -n/3$, $n$ being the dimension of the defect). The first dynamical scalar field models proposed were of the kind of quartic, quadratic and exponential scalar field (see, for example: Bronstein 1933; Ozer & Taha 1987; Freese et al. 1987; Frieman et al. 1995; Wetterich 1995; Bloomfield-Torres & Waga 1996; Coble et al. 1996; Cadwell et al. 1998), but more recently, they have been proposed models which consider potentials which, for a wide range of initial conditions, make the scalar fields to settle into a "tracking solution" that depends only upon one parameter and the evolution of the cosmic scale factor (Wetterich 1988; Ratra & Peebles 1988; Zlatev et al. 1999).

In this work we will try to find out if it is possible to discriminate dark energy models from the effects that they produce in the growth of matter perturbations and formation of clusters of galaxies. For the sake of simplicity, instead of dealing with a lot of dark energy models to derive general conclusions, we have chosen a simple model which shows a great number of different behaviours. Thus, for our study, we will use an hydrodynamical dark energy model whose equation of state fulfills $\omega = p_x/\rho_x = \omega_0 \rho_x^{\gamma-1}$, with $\omega_0 < 0$ and $\gamma > 0$ (Aguerri & Membrado 1999). It can be seen that depending on the values of $\gamma$, our models are $\omega$ strongly and/or slowly varying, $\omega$-constant models as those proposed by Steinhardt (1996) and Turner & White (1997), and cosmological constant models. The chosen model is physically equivalent, for zero curvature, to a fluid with bulk viscosity $\eta(\rho) = -(\omega_0/\sqrt{3})(\rho)^{\gamma-1/2}$ (Barrow 1988; Lydsey 1994), and a perfect fluid with $\beta = 1$, for which, the dark energy fulfills $p = \left[(\beta - 1) + \omega_0 \rho^{\gamma-1}\right] \rho$.

In Sect. 2, we propose our cosmological background model for flat universe. In Sect. 3, we deal with linear perturbation theory. Sections 4 and 5 are devoted to the spherical infall model. Finally, in Sect. 6, we present our conclusions.

Article published by EDP Sciences and available at http://www.aanda.org or http://dx.doi.org/10.1051/0004-6361:20034107

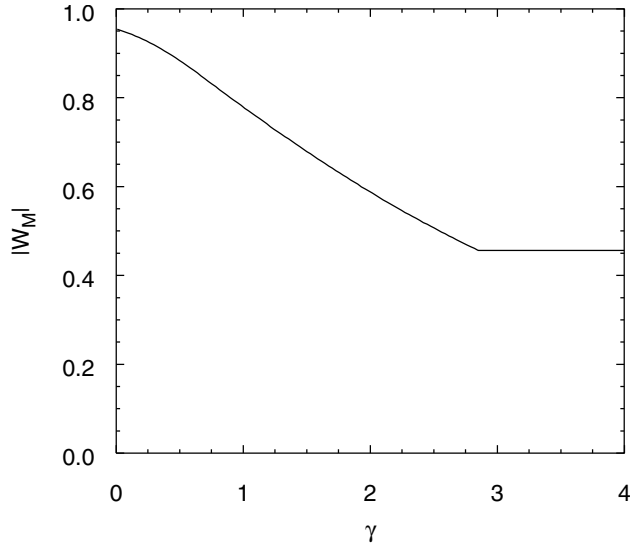


**Fig. 1.** Constraints for the parameters $\gamma$ and $W$ ($\mid W(\gamma) \mid > \mid W_M(\gamma) \mid$) based upon WMAP and other data; the constraint shown by the horizontal line is based upon the observational fact that the expansion of the Universe is speeding up at present.

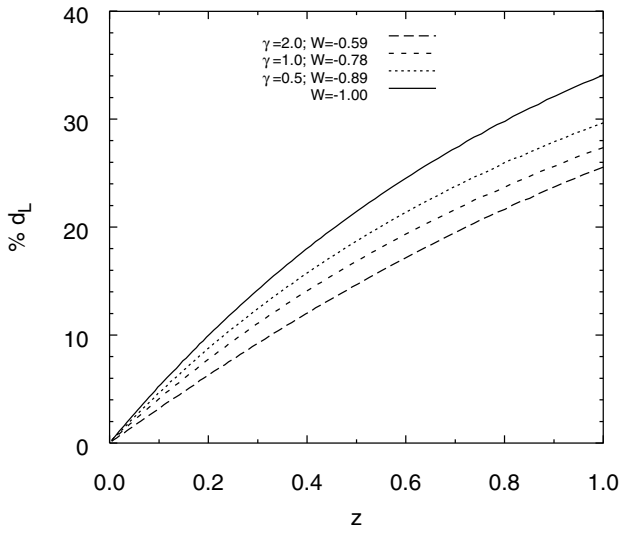


**Fig. 2.** Comparisons among luminosity distances derived from $\Omega_{\rm m0} = 0.27$ dark energy models (we have taken $W = W_M(\gamma)$ for each $\gamma$) and the $\Omega_{\rm m0} = 1$ model: $\%\, d_L = 100 \left[ \frac{{\rm d}_{L_{\Omega_{\rm m0},\gamma,W}}}{{\rm d}_{L_{\Omega_{\rm m0}=1}}} - 1 \right]$.

## 2. The cosmological background model

We will consider a cosmological background of flat universe composed by non-relativistic matter, radiation and dark energy (hereafter: subindex 0 will represent magnitudes at present; magnitudes with a bar, will represent background magnitudes). In this work we will deal with an equation of state for dark energy of the kind $\omega_x = \frac{\bar{p}_x}{\bar{\rho}_x} = W\left(\frac{\bar{\rho}_x}{\bar{\rho}_{x0}}\right)^{\gamma-1}$, i.e., an energy density, $\bar{\rho}_x$, which evolves as (Aguerri & Membrado 1999)

$$\bar{\rho}_x = \bar{\rho}_{x0} \begin{cases} \left[ (1+W) \left(\frac{a}{a_0}\right)^{-3(1-\gamma)} - W \right]^{1/(1-\gamma)}, & \gamma \neq 1\,, \\ \left(\frac{a}{a_0}\right)^{-3(1+W)}, & \gamma = 1. \end{cases} \quad (1)$$

$a$ being the expansion parameter. Equation (1) together with the fact that $\omega_x = 1-(1+W)\left[\frac{\Omega_{\rm m0}(1-\Omega_{\rm m})}{\Omega_{\rm m}(1-\Omega_{\rm m0})}\right]^{\gamma-1}$ (radiation is neglected, i.e., $\Omega_{\rm m} = \frac{\bar{\rho}_{\rm m}}{\bar{\rho}_{\rm m}+\bar{\rho}_x}$) inform us about the behaviours of the model. Thus, for $\gamma < 1$, as energy density behaves, at $\frac{a}{a_0} \ll 1$, like matter does, and like cosmological constant when $\frac{a}{a_0} \gg 1$, $\omega$ is not slowly varying (it does not fulfill $|{\rm d}\omega/{\rm d}\Omega| \ll 1/(1-\Omega)$; see Wang & Steinhardt 1998); for $\gamma > 1$, only when matter dominates (for $\frac{a}{a_0} \ll 1$, the energy density of dark energy is a constant), the model is slowly varying; finally, $\gamma = 1$ models (proposed by Steinhardt 1996; Turner & White 1997), and $W = -1$ models (cosmological constant) are $\omega$-constant models.

To estimate the range of allowed values for $W$ and $\gamma$, we will use the constraints derived by Spergel et al. (2003) based upon a combination of WMAP data with other finer scale *CMB* experiments (*ACBAR* and *CBI*), *2dFGRS* measurements, and Lya forest data. Thus, defining $\omega_{\rm eff} = \int {\rm d}a\Omega_x(a)\omega(a) / \int {\rm d}a\Omega_x(a)$ (Huey et al. 1999), we will assume $\omega_{\rm eff} < -0.78$ and $\Omega_{\rm m0} = 0.27 \pm 0.04$. In Fig. 1, $|W_M(\gamma)|$, fulfilling $\omega_{\rm eff}(W_M(\gamma), \gamma) = -0.78$, is plotted, so values of $|W|$ greater than $|W_M(\gamma)|$ are allowed (it is not observed any dependence on $\Omega_{\rm m0}$). Another constraint comes from imposing that the Universe is speeding up, at present (see, for example: Perlmutter et al. 1997, 1999; Schmidt et al. 1998). Thus, our models predict an accelerate expansion, for $|W| > |W_E| = \frac{1}{3(1-\Omega_{\rm m0})}$, where $W_E$, corresponds to the value of $W$ for which $\frac{{\rm d}\ddot{a}}{{\rm d}a}\Big|_{a=a_0} = 0$. The horizontal line in Fig. 1 shows $|W_E|$ for $\Omega_{\rm m0} = 0.27$.

An observational difference among models with and without dark energy comes from luminosity distances, $d_L$, to sources at different redshifts $z$ (Goobar et al. (2002), in their Monte-Carlo package for simulated high-redshift supernova data, SNOC, developed a generator of luminosity distances for any $\omega_x(z)$; so, our models are also included). Taking into account that $d_L = \frac{c}{H_0}(1+z)\int_0^z \sqrt{\frac{\bar{\rho}_0}{\bar{\rho}}}{\rm d}z$, with $H = \frac{\dot{a}}{a}$ and $z = -1 + a_0/a$, it is straightforward to derive, for redshifts $z \ll 1$:

$$\frac{H_0 d_L}{c} \approx z + \frac{z^2}{4}\left[1 - 3W(1-\Omega_{\rm m0})\right] + z^3\left[-\frac{7}{8} + \left(\frac{5}{8} + G_{\gamma,W}\right)(1-\Omega_{\rm m0})\right] + O\left(z^4\right); \quad (2)$$

where

$$G_{\gamma,W} = \begin{cases} \frac{3}{2} - \frac{1}{4}(1+W)\left[3(1-\gamma) + \frac{1}{1-\gamma} - \frac{1}{2}\right], & \gamma \neq 1; \\ \frac{3}{2} - \frac{1}{4}(1+W)\left[3(1+W) + \frac{1}{2}\right], & \gamma = 1. \end{cases} \quad (3)$$

We notice that the $z^2$ term of Eq. (2) does not depend on $\gamma$, while the $z^3$ term depends on both $W$ and $\gamma$. This makes the acceleration parameter, $q_0 = -\left(\frac{\ddot{a}a}{\dot{a}^2}\right)_{a=a_0}$, to depend only on $W$. As $q_0 = (1 + 3W\Omega_{x0})/2$, the cosmological constant models ($W = -1$) show the smallest $q_0$. A comparison among luminosity distances is shown in Fig. 2. In this figure, it is seen that the differences among models grow as the redshift is greater. It can be noticed that the greatest difference corresponds to the cosmological constant model, being difficult to distinguish

among $W \neq -1$ models. In this sense, Maor & Brustein (2003) have shown that various scalar field models of dark energy predict a degenerate luminosity distance and thus cannot be distinguished by supernovae measurements alone; CMB anisotropy measurements does not reduce significantly the degeneracy.

## 3. Linear growth of matter perturbations

In this section we will assume that non-relativistic matter is slightly perturbed from the cosmological background proposed in the previous section, in a region where Newtonian approximation can be applied (a small region compared to the Hubble length $c/H$). We will only deal with growing modes of matter perturbations. Therefore, our results are only valid from redshifts where the decaying modes of perturbations have decayed and the velocity field have reached the amplitud given by linear theory. In this work we denote: $\delta(\boldsymbol{x}, a) = \frac{\rho_{\rm m}(\boldsymbol{x},a)-\bar{\rho}_{\rm m}(a)}{\bar{\rho}_{\rm m}(a)}$ as the dimensionless density contrast at expansion parameter $a$ and expanding coordinate $\boldsymbol{x}$, comoving in the background model ($\boldsymbol{r} = a\boldsymbol{x}$; $\boldsymbol{r}$ being the proper distance from some chosen origin); and, $\boldsymbol{v} = a\dot{\boldsymbol{x}}$, as the peculiar velocity of the matter component (related with the proper velocity, $\boldsymbol{u} = \dot{\boldsymbol{r}}$, by $\boldsymbol{u} = \dot{a}\boldsymbol{x} + \boldsymbol{v}$).

We have observed that perturbations in the dark energy component, $\delta_x$, are much smaller than $\delta$ (Membrado 2004), so they will not be treated in this work. To deal with such perturbations we have used the scalar field representation. Superhorizon-sized perturbations at early times fulfill $\frac{\delta_x}{\delta} \propto \left(\frac{a}{a_0}\right)^{3(\gamma-1)}$ for $\gamma > 1$ (at early times, $\gamma > 1$ models behave as a cosmological constant with negligible perturbations), and $\delta_x$ represents about 10% of $\delta$ for $\gamma \leq 1$. After reaching a maximum, $\delta_x$ decreases and takes negative values. In $\gamma < 1$ models, $\delta_x$ shows also a minimum, so $\mid \delta_x \mid$ decreases up to the present ($\gamma < 1$ models tend to a cosmological constant at later times). Our studied models show that $\delta_x$ is negligible at present for small scale perturbations and is about 1% of $\delta$ for large scale perturbations.

Taking into account the above assumptions, the linearized equation for the growth of matter perturbations is given by

$$\frac{\bar{\rho}}{\bar{\rho}_0}a^2\frac{\partial^2\delta}{\partial a^2} + \left[3\frac{\bar{\rho}}{\bar{\rho}_0} + \frac{1}{2}\frac{a}{\bar{\rho}_0}\frac{{\rm d}\bar{\rho}}{{\rm d}a}\right]a\frac{\partial\delta}{\partial a} = \frac{3}{2}\Omega_{\rm m0}\left(\frac{a}{a_0}\right)^{-3}\delta, \tag{4}$$

where $\Omega_{\rm m0} = \bar{\rho}_{\rm m0}/\bar{\rho}_0$. As we are interested in the growing solution, we can consider that $\delta(\boldsymbol{x}, a) = A(\boldsymbol{x})\frac{\delta_{\rm g}(a)}{\delta_{\rm g}(a_0)}$, where $\frac{\delta_{\rm g}(a)}{\delta_{\rm g}(a_0)}$ is the growing solution of Eq. (4) with value equal to the unity at present ($A(\boldsymbol{x})$ can be calculated from the power spectrum of $\delta$). With respect to the the radial peculiar velocity, $v$ is given by (for the growing mode in a spherical collapse)

$$v = -\frac{1}{3}f_{\rm g}H\Delta a x. \tag{5}$$

In this last equation, $\Delta(x, a)$ is the average density contrast inside $x$, i.e.,

$$\Delta(x, a) = \frac{3}{x^3}\int_0^x \delta(x', a)x'^2{\rm d}x', \tag{6}$$

and $f_{\rm g}$ being the growth index given by

$$f_{\rm g} = \frac{a}{\delta_{\rm g}}\frac{{\rm d}\delta_{\rm g}}{{\rm d}a}, \tag{7}$$

(Eqs. (4) and (5) can be derived from the standard equations for an ideal fluid with zero pressure; see, for example, Peebles 1980).

It is easy to derive the asymptotic growing solutions of Eq. (4), which can be used as boundary conditions to integrate such an equation. For $a \ll a_{\rm eq}$, the asymptotic solutions are given by:

$$\delta_{{\rm g}_{\gamma<1}} \propto 1 + \frac{3}{2}\frac{a}{a_{\rm eq}} - \frac{9}{16}\frac{\Omega_{x0}}{\Omega_{\rm m0}}(1+W)^{\frac{1}{1-\gamma}}\left(\frac{a}{a_{\rm eq}}\right)^2 + \ldots; \tag{8}$$

$$\delta_{{\rm g}_{\gamma=1}} \propto 1 + \frac{3}{2}\frac{a}{a_{\rm eq}} - \frac{9}{4}\frac{\Omega_{x0}}{\Omega_{\rm m0}}\frac{1-W}{(2-3W)^2}\left(\frac{a_0}{a_{\rm eq}}\right)^{3W}\left(\frac{a}{a_{\rm eq}}\right)^{2-3W} + \ldots; \tag{9}$$

$$\delta_{{\rm g}_{\gamma>1}} \propto 1 + \frac{3}{2}\frac{a}{a_{\rm eq}} - \frac{9}{50}\frac{\Omega_{x0}}{\Omega_{\rm m0}}(-W)^{\frac{1}{1-\gamma}}\left(\frac{a_0}{a_{\rm eq}}\right)^{-3}\left(\frac{a}{a_{\rm eq}}\right)^5 + \ldots; \tag{10}$$

where $a_{\rm eq}/a_0 = \Omega_{r0}/\Omega_{\rm m0}$, $\Omega_{r0} = \bar{\rho}_{r0}/\bar{\rho}_0$, and $\Omega_{x0} = \bar{\rho}_{x0}/\bar{\rho}_0$. Equations (8)–(10) tell us that when radiation dominates ($a \ll a_{\rm eq}$), the effects of dark energy does not appear neither at zero nor at first order.

Taking into account that for the $\Omega_{\rm m0} = 1$ model, $\delta_{\rm g} \propto 1 + \frac{3}{2}\frac{a}{a_{\rm eq}}$, and $f_{\rm g} = \frac{3}{2}\frac{a}{a_{\rm eq}}\left[1 + \frac{3}{2}\frac{a}{a_{\rm eq}}\right]^{-1}$ (see, for example: Mészáros 1974; Groth & Peebles 1975), we show, in Fig. 3, a comparison among some models with respect to the density contrast, $\delta_{\rm g}$, and the growth index, $f_{\rm g}$, at redshitfs smaller than $z = 1000$ (at these redshifts, the decaying modes of perturbations have decayed away). It can be seen that, up to $z = 1$, the models show noticeable different $\delta_{\rm g}$ behaviours. With respect to $f_{\rm g}$ the differences are not too large up to $z = 1$; from this redshift, dark energy models differ clearly from the $\Omega_{\rm m0} = 1$ model, but it is very difficult to distinguish among $\gamma$, $W$ models. At $z = 0$, we obtain $f_{\rm g} = 0.48 \pm 0.04$ for $\Omega_{\rm m0} = 0.27 \pm 0.04$. This is a good agreement with the value obtained by the 2dF group; they found that $f = 0.46$ for $\Omega_{\rm m0} = 0.27$ (Hawkins et al. 2003). Thus, theoretically, $\Omega_{\rm m0}$ could be discriminated from observational values of $f_{\rm g}(0)$. However, as the bias parameter is unknown at present, the only observational restriction is $f_{\rm g} \geq 0.4$ (see, for example: Yahil 1985; Lynden-Bell et al. 1989; Strauss 1989; Yahil et al. 1991; Dekel et al. 1990; Yahil 1990; Bertschinger 1990; Kaiser et al. 1991). Wang & Steinhardt (1998), from the linearized equation for the growth of matter perturbations and for slowly varying equations of state of dark energy, derived an analytical expression for $f$ (for a review of the case of a constant equation of state, see, for example, Lokas 2001). They showed that $f = \Omega_{\rm m}^{\alpha}$, $\alpha$ depending on $\omega_x$ and weakely on $\Omega_{\rm m}$. Our results for $f_{\rm g}(z = 0)$ can be fitted by $f_{\rm g}(z = 0) = \Omega_{\rm m0}^{0.63+0.06W-0.07\Omega_{\rm m0}}$ (notice that this fitting function does not depend on $\gamma$; this is a consequence of the fact that for our models $\rho_x(z \to 0) = \rho_{x0}[1 + 3(1 + W)z + ...]$, so the dependence on $\gamma$ appears at orders greater than the first one). Overall it is accurate within 0.4%; with respect to the analytical expression by Wang & Steinhardt (1998), our expression is accurate within 0.9%.

A special mention should be made about the product $f_{\rm g}(z)\frac{H(z)}{H_0}$, which, for the $\Omega_{\rm m0} = 1$ model, takes the value $f_{\rm g}\frac{H(z)}{H_0} = \frac{3}{2}\frac{a_0^3}{a_{\rm eq}a^2}\left[1 + \frac{3}{2}\frac{a}{a_{\rm eq}}\right]^{-1}$. We have noticed that this product

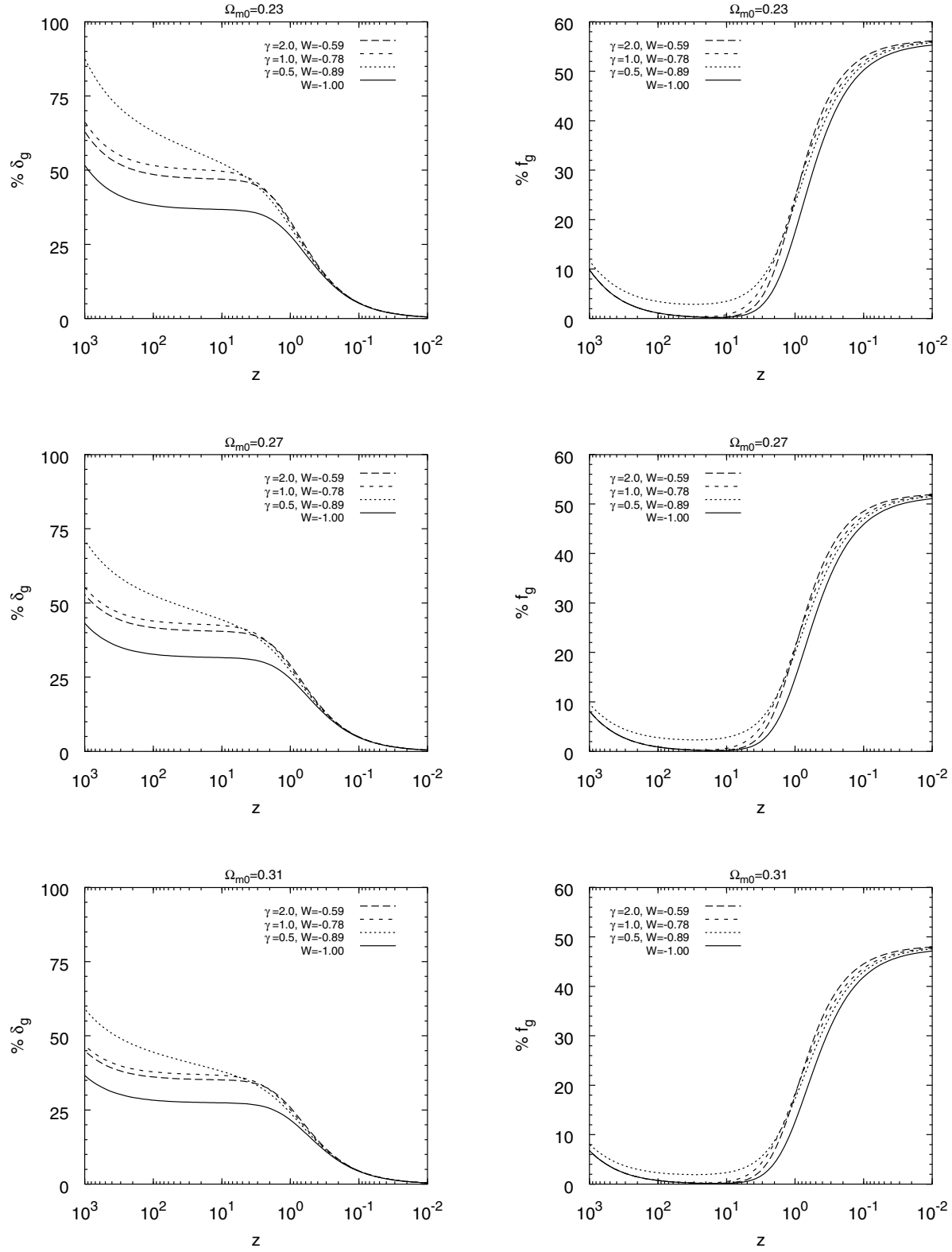


**Fig. 3.** Comparisons of density contrast, $\delta_g$, and growth index, $f_g$, among some different dark energy models: $\%\delta_g(z) = 100\left[\frac{\delta_{g\Omega_{m0},\gamma,W}(z)/\delta_{g\Omega_{m0},\gamma,W}(0)}{\delta_{g\Omega_{m0}=1}(z)/\delta_{g\Omega_{m0}=1}(0)} - 1\right]$; $\%f_g = 100\left[1 - \frac{f_{g\Omega_{m0},\gamma,W}}{f_{g\Omega_{m0}=1}}\right]$.

has the main dependence on the value of $\Omega_{m0}$, being very low the depende on $\gamma$ an $W$ (see Fig. 4). Lahav et al. (1991) noticed a similar behaviour when dealing with cosmological constant models; they named it "fH conspiracy". The main consequence of this conspiracy is that, according to Eq. (5), the peculiar velocity dependens on $\gamma$ and $W$ from the average density contrast.

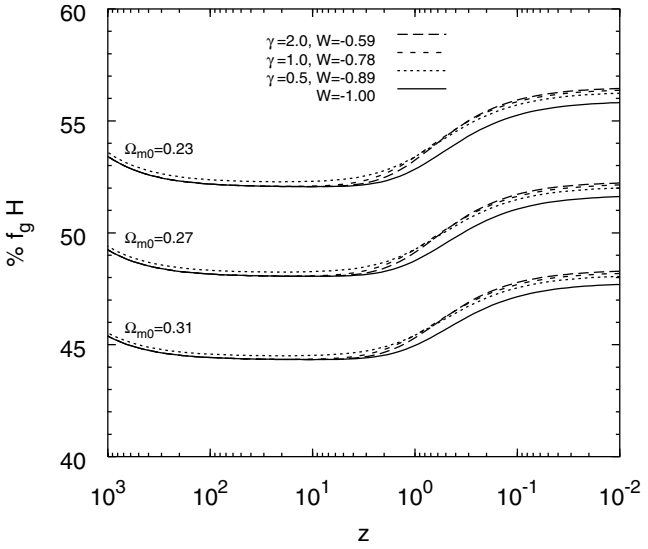


**Fig. 4.** $\%f_{\rm g}H = 100\left[1-\frac{[f_{\rm g}H]_{\Omega_{\rm m0},\gamma,W}}{[f_{\rm g}H]_{\Omega_{\rm m0}=1}}\right]$, for the cosmological background models of Fig. 3.

## 4. The spherical infall model

### 4.1. Motion equation of a collapsing spherical shell

The collapse of spherical shells has been discussed extensively in the literature. Gunn & Gott (1972) applied it to density and velocity field around clusters of galaxies, assuming just matter; Peebles (1984) and Weinberg (1987) studied it in the case of a flat universe with matter and cosmological constant, while Lahav et al. (1991) studied it for the three kinds of universes.

We will start our study from the equation of motion of a collapsing spherical shell of matter in a background of matter, radiation and dark energy. Assuming that no other mass shell crosses such a shell, the equation of motion can be derived from $\ddot{r} = -\frac{{\rm d}\phi}{{\rm d}r}$ ($\phi$ is the gravitational potential fulfilling $\nabla^2\phi = \frac{4\pi G}{c^2}\left[\rho_{\rm m} + (\bar{\rho}_r + \bar{\rho}_x) + 3(\bar{p}_r + \bar{p}_x)\right]$), i.e.,

$$\ddot{r} = -\frac{G}{r^2}\mathcal{M} - \frac{4\pi G}{3c^2}\left[(\bar{\rho}_r + \bar{\rho}_x) + 3(\bar{p}_r + \bar{p}_x)\right] r. \tag{11}$$

In Eq. (11), $\mathcal{M}$ is the mass of the shell (it is constant in the collapse). For a shell which at $t_i$ has a radius $r_i = \frac{a_0 x_i}{1+z_i}$, $\mathcal{M}$ is given by (it is assumed that linear theory of perturbations can be applied at $t_i$),

$$\mathcal{M}(r_i, t_i) = \frac{4\pi}{c^2}\bar{\rho}_{\rm m}(t_i)\frac{r_i^3}{3}\left[1 + \Delta(x_i, t_i)\right]. \tag{12}$$

Defining, for any time, the radius of the shell as

$$r(x_i, t) = \frac{A(x_i, t)a_0 x_i}{1 + z_i}, \tag{13}$$

and taking derivatives with respect to $a$, Eq. (11) reads as

$$a^2\frac{\bar{\rho}}{\bar{\rho}_0}A'' = -aA'\left[\frac{\bar{\rho}}{\bar{\rho}_0} + \frac{1}{2}a\frac{\bar{\rho}'}{\bar{\rho}_0}\right] - \frac{1}{2A^2}\frac{\bar{\rho}}{\bar{\rho}_0}[1 + \Delta(x_i, a_i)] - \frac{A}{2}\left[\frac{\bar{\rho}_r + \bar{\rho}_x}{\bar{\rho}_0} + 3\frac{\bar{p}_r + \bar{p}_x}{\bar{\rho}_0}\right]. \tag{14}$$

This equation must be solve with the boundary conditions

$$A(x_i, a_i) = 1, \tag{15a}$$

$$A'(x_i, a_i) = \frac{1}{a_i}\left[1 - \frac{1}{3}f_{\rm g}(a_i)\Delta(x_i, a_i)\right], \tag{15b}$$

coming from Eqs. (13) and (5).

To evaluate $\Delta(x_i, a_i)$ from Eq. (6), we need to know the profile of the collapsing structure at $a_i$. For a peak with height $\eta$ of its maximum (the height of a peak, $h(z)$, can be expressed in units of the rms fluctuations of the density field $\sigma_0(z)$, i.e., $h(z) = \eta\sigma_0(z)$), we use the results derived from the work of Bardeen et al. (1986; hereafter *BBKS*)

$$\delta(x, z) = \frac{\sigma_0(z)}{2\pi^2}\int_0^\infty k^2\frac{P_k(z)}{\sigma_0^2(z)}\left[\frac{\eta - \xi^2\eta - \xi\chi}{1-\xi^2} - \frac{\chi R_\star^2 k^2}{3\xi(1-\xi^2)}\right] \times \frac{\sin\, kx}{kx}{\rm d}k; \tag{16}$$

where

$$R_\star = \sqrt{3}\frac{\sigma_1}{\sigma_2},\ \ \xi = \frac{\sigma_1^2}{\sigma_2\sigma_1},\ \ \sigma_i^2(z) = \frac{1}{2\pi^2}\int_0^\infty P_k(z)k^{2+2i}{\rm d}k,$$

$$\chi = \frac{3(1-\xi^2) + (1.216 - 0.9\xi^4)\,{\rm e}^{-\xi/2(\xi\eta/2)^2}}{[3(1-\xi^2 + 0.45 + (\xi\eta/2)^2]^{1/2} + \xi\eta/2}. \tag{17}$$

For $P_k$, we could take the cold dark matter power spectrum ($\delta(x, z)$ is expressed as a superposition of modes, $\delta_k(z)$, with diferent wavenumbers $k$); however, as there is not a natural cut-off for hight wavenumber in such a spectrum, we will make use of a Gaussian filter and will take

$$P_k = P_0 \mid \delta_{\rm g}(z)/\delta_{\rm g}(0) \mid^2 kT_{\boldsymbol{k}}^2\ {\rm e}^{-(R_f k)^2};\ R_f = 3\ h^{-1}\,{\rm Mpc}. \tag{18}$$

In this last equation, $k$ is proportional to the initial spectrum taken as the Zeldovich spectrum that arises in inflation, and $T_k^2$ is the transfer function for linear perturbations at late times. $T_k^2$ is given, for cold dark matter (adiabatic fluctuations), by the following numerical fitting formulae of *BBKS* (time independent in the range of $z$'s considered in this study):

$$T_{\boldsymbol{k}}^2 = \frac{[\ln(1 + 2.34q)/(2.34q)]^2}{[1 + 3.89q + (16.1q)^2 + (5.46q)^3 + (6.71q)^4]^{1/2}};$$

$$q = \left(\frac{k}{{\rm Mpc}^{-1}h}\right)\frac{1}{\Gamma};\ \ \Gamma = h\Omega_{\rm m0}\exp\left[-\Omega_{B0}\left(1 + \sqrt{2h}/\Omega_{\rm m0}\right)\right] \tag{19}$$

$\Gamma$ was originally defined by Efstathiou et al. (1992) for $\Omega_{\rm m0} = 1$ and generalized for $\Omega_{\rm m0} \neq 1$ by Sugiyama (1995). From a combination of WMAP data with other finer scale *CMB* experiments (*ACBAR* and *CBI*), *2dFGRS* measurements, and Lya forest data (Spergel et al. 2003), we assume $h = 0.71^{+0.04}_{-0.03}$ and $\Omega_{B0} = \bar{\rho}_{B0}/\bar{\rho}_0 = 0.044 \pm 0.004$. In Eq. (18), $P_0$ can be determined from the present rms density fluctuations in the sphere with a radius $R = 8\ h^{-1}$ Mpc, $\sigma_8$, given by

$$\sigma_8^2 = \int_0^\infty k^2\frac{P_0 kT_{\boldsymbol{k}}^2}{2\pi^2}\left[\frac{3(\sin\, kR - kR\,\cos\, kR)}{(kR)^3}\right]^2{\rm d}k. \tag{20}$$

$\sigma_8$ can be derived by fitting the theoretically predicted number density of clusters versus temperature (cumulative temperature function) to the observed X-ray cluster abundance as a function of temperature. In Sect. 4.4 we will see that our results

for $\sigma_8$ can be fit by $\sigma_8 = 0.49\Omega_{m0}^{0.04W-0.22\Omega_{m0}-0.31}$; overall it is accurate within 0.5%. Using data from COBE and 2dF, Lahav et al. (2002) obtained the value of $\sigma_8$ assuming $\Omega_{m0} = 0.3$ and $W = -1$; the value obtained from our parametrization of $\sigma_8$ is within the 95% CL of their measurements.

Therefore, fixed a height of a peak, $\eta$, chosen a shell, $x_i$, and calculated $\Delta(x_i, a_i)$, the integration of Eq. (14) can be developed. We will begin the integration at $z_i = 1000$, which is a relatively shortly epoch after recombination when the growth of perturbations is fully given by linear theory and late enough for the decaying modes of perturbations to have decayed away and for the velocity field to have reached the amplitud given by linear theory, irrespective of initial velocities. Ones $A(x_i, z)$ is calculated for the shell enclosing a mass $\mathcal{M}$ given by Eq. (12), we can know the radius, $r(x_i, z)$, from Eq. (13), the proper velocity, $u = \frac{dr}{dt}$, from

$$u(x_i, a) = H(a)r(x_i, a)a\frac{A'(x_i, a)}{A(x_i, a)}, \tag{21}$$

and the peculiar velocity, $v = u - Hr$, from

$$v(z) = H(z)r(x_i, z)\left[a\frac{A'}{A} - 1\right]. \tag{22}$$

For a shell, enclosing a mass $\mathcal{M}$, its proper velocity decreases up to it reaches a value equal to zero at the turn-around radius, $R_{TA}$, when $t = t_{TA}$. From this point, the radius of the shell begins to decrease. The collapse finishes when a virialized structure with radius $R_{VIR}$ is formed at $t = t_{VIR} \approx 2t_{TA}$ (clusters formally collapse to $r = 0$ according to an unperturbed spherical solution). As Eq. (14) is not able to study virial processes, we have studied the evolution of the shell up to the turn-around point. Then, in order to derive $R_{VIR}$, we have applied the conservation of the energy at $R_{TA}$ and at $R_{VIR}$. At $R_{TA}$ we have assumed that the sphere inside the shell is an homogeneus one, while at $R_{VIR}$, a singular isothermal sphere is taken (Cole & Lacey 1996, show that a singular isothermal sphere is a very good approximation when relating the mass contained within the virial radius to the velocity dispersion).

### 4.2. Relation between $R_{TA}$ and $R_{VIR}$

To estimate $R_{VIR}$ we will impose the conservation of the energy, $E$, which will be calculated at $R_{TA}$ and at $R_{VIR}$. At the turn-around point, the kinetic energy, $K$, is zero, so we have only to calculate the potential energy, i.e., $E = E_p(R_{TA})$. At $R_{VIR}$, the kinetic energy will be calculated imposing the virial theorem under steady conditions.

It is well known that a $\delta\rho_m(\boldsymbol{r})$ changes the potential energy according with $\delta E_p = \frac{1}{c^2}\int \delta\rho_m(\boldsymbol{r})\phi(\boldsymbol{r})d\boldsymbol{r}$, and as $\delta\rho_m(\boldsymbol{r})$ modifies only the gravitational potential due to matter, $\phi_m(\boldsymbol{r})$, the potential energy, $E_p$, is (see, for example, Binney & Tremaine 1994)

$$E_p = \frac{1}{2c^2}\int \rho_m(\boldsymbol{r})\phi_m(\boldsymbol{r})d\boldsymbol{r} + \frac{1}{c^2}\int \rho_m(\boldsymbol{r})\left[\phi(\boldsymbol{r}) - \phi_m(\boldsymbol{r})\right]d\boldsymbol{r}. \tag{23}$$

Thus, assuming a matter sphere of mass $\mathcal{M}$ and radius $R$, with constant density, for which $\phi_m(r) = -\frac{3}{2}\frac{G\mathcal{M}}{R} + \frac{1}{2}\frac{Gm(r)}{r}$, and $\phi(r) - \phi_m(r) = \frac{2\pi G}{3c^2}\left[(\bar{\rho}_r + \bar{\rho}_x) + 3(\bar{p}_r + \bar{p}_x)\right]r^2$, the potential energy reads as

$$E_p(R) = -\frac{3G\mathcal{M}^2}{5R}\left[1 - \frac{2\pi R^3}{3\mathcal{M}c^2}\zeta\right], \tag{24}$$

with

$$\zeta = \left[(\bar{\rho}_r + \bar{\rho}_x) + 3(\bar{p}_r + \bar{p}_x)\right], \tag{25}$$

and therefore, at $a = a_{TA}$,

$$E = -\frac{3G\mathcal{M}^2}{5R_{TA}}\left[1 - \frac{2\pi R_{TA}^3}{3\mathcal{M}c^2}\zeta_{TA}\right]. \tag{26}$$

For the virialized structure, we take a singular isothermal sphere. In this case, to calculate the potential energy due to matter is better to use the trace of the potential energy tensor of Chandrasekhar (see, for example, Binney & Tremaine 1994). Thus,

$$\begin{aligned} E_p &= -\frac{1}{c^2}\int \rho_m(\boldsymbol{r})\boldsymbol{r}\cdot\boldsymbol{\nabla}\phi_m(\boldsymbol{r})d\boldsymbol{r} \\ &\quad + \frac{1}{c^2}\int \rho_m(\boldsymbol{r})\left[\phi(\boldsymbol{r}) - \phi_m(\boldsymbol{r})\right]d\boldsymbol{r}. \end{aligned} \tag{27}$$

Assuming $\rho_m \propto 1/r^2$, and taking $\frac{d\phi_m(r)}{dr} = \frac{G}{r^2}\mathcal{M}$ (see Eq. (11)), it is then derived that

$$E_p(R_{VIR}) = -\frac{G\mathcal{M}^2}{R_{VIR}}\left[1 - \frac{2\pi R_{VIR}^3}{9\mathcal{M}c^2}\zeta_{VIR}\right]. \tag{28}$$

The Virial Theorem for the virialized structure can be derived from the Jeans equations (see for example, Binney & Tremaine 1994). For our case, this theorem reads as $\int_0^{R_{VIR}} r^3\frac{d\rho_m\sigma_{los}^2}{dr}dr + \int_0^{R_{VIR}} r^3\rho_m\frac{d\phi}{dr}dr = 0$, where $\sigma_{los}^2 = \frac{\langle V_{VIR}^2\rangle}{3}$, $\sigma_{los}$ and $\langle V_{VIR}^2\rangle$ being the line-of-sight velocity dispersion and the mean square velocity of particles in the cluster. Thus,

$$\sigma_{los}^2 = \frac{G\mathcal{M}^2}{2R_{VIR}}\left[1 + \frac{4\pi R_{VIR}^3}{9\mathcal{M}c^2}\zeta_{VIR}\right] \tag{29}$$

(it should be noticed that a surface term appears in the integration of the first term of the Virial Theorem). The Kinetic energy is then calculated from the trace of the kinetic energy tensor, i.e., $K = \frac{3}{2}\sigma_{los}^2\mathcal{M}$, so

$$K = \frac{3G\mathcal{M}^2}{4R_{VIR}}\left[1 + \frac{4\pi R_{VIR}^3}{9\mathcal{M}c^2}\zeta_{VIR}\right]. \tag{30}$$

Therefore, at $a = a_{VIR}$,

$$E = -\frac{G\mathcal{M}^2}{4R_{VIR}}\left[1 - \frac{20\pi R_{VIR}^3}{9\mathcal{M}c^2}\zeta_{VIR}\right]. \tag{31}$$

Finally, defining $\rho_{c_{TA}} = \frac{3\mathcal{M}c^2}{4\pi R_{TA}^3} = \frac{\bar{\rho}_m(a_i)[1+\Delta(x_i,a_i)]}{A^3(x_i,a_{TR})}$, and imposing the conservation of the energy, it is derived that

$$1 = \frac{6}{5}\left(2 - \frac{\zeta_{TA}}{\rho_{c_{TA}}}\right)\left(\frac{R_{VIR}}{R_{TA}}\right) + \frac{5}{3}\frac{\zeta_{VIR}}{\rho_{c_{TA}}}\left(\frac{R_{VIR}}{R_{TA}}\right)^3. \tag{32}$$

Other authors, as Lahav et al. (1991), Wang & Steinhardt (1998) and Battye & Weller (2003), derived similar expressions to Eq. (32), but assuming constant density for the virial structure. When assuming constant density, the potential energy, $E_p$,

is given by Eq. (24), and the kinetic energy from the virial theorem $2K + E_{\rm p} = 0$. Thus, $E = -\frac{3G\mathcal{M}^2}{10R_{\rm VIR}}\left[1 - \frac{8\pi R_{\rm VIR}^3}{3\mathcal{M}c^2}\zeta_{\rm VIR}\right]$, and imposing the conservation of the energy, $1 = \left(2 - \frac{\zeta_{\rm TA}}{\rho_{c_{\rm TA}}}\right)\left(\frac{R_{\rm VIR}}{R_{\rm TA}}\right) + 2\frac{\zeta_{\rm VIR}}{\rho_{c_{\rm TA}}}\left(\frac{R_{\rm VIR}}{R_{\rm TA}}\right)^3$. When cosmological constant is consider ($\bar{\rho}_x = -\bar{p}_x$), and radiation contribution is neglected, the result by Lahav et al. (1991) is reproduced. By assuming $\frac{R_{\rm VIR}}{R_{\rm TA}} \approx \frac{1}{2} + \epsilon$, with $\epsilon \ll 1$, and $\bar{p}_x = W\bar{\rho}_x$, the results by Wang & Steinhardt (1998) and Battye & Weller (2003) are reproduced. However, when assuming constant density for the virialized cluster, $\sigma_{\rm los}^2$ changes to about 40% our proposed value; so, the results by Lahav et al. (1991), Wang & Steinhardt (1998) and Battye & Weller (2003) are not useful for our purpose.

In Fig. 5, we show virial angular radii, $\theta_{\rm VIR}$, for $\sigma_{\rm los} = 750$ and 1000 spherical clusters at redshifts from $z = 0.01$ until $z = 0.1$, under several cosmologies. We notice that the greater the $\Omega_{\rm m0}$ and the $\gamma$ are, the smaller the $\theta_{\rm VIR}$ is. We also see that $\theta_{\rm VIR}(\gamma < 1)$ is close to $\theta_{\rm VIR}(W = -1)$; this is due to the behaviour of the dark energy density for $\gamma < 1$ models at small redshifts.

### 4.3. Mass-temperature relation

As observations directly determine the X-ray tempeture of the cluster gas instead of the mass of the cluster, it is interesting to derive the mass-temperature relation. This one can be obtained from the virial theorem.

The observed temperature of the gas is

$$K_{\rm B}T = \frac{\mu {\rm m_p}}{\beta}\sigma_{\rm los}^2; \tag{33}$$

where $K_{\rm B}$ is the Boltzmann constant; $\mu$ the mean molecular weigth (0.59); and $m_{\rm p}$, the mass of the proton. Thus, taking $\sigma_{\rm los}^2$ from Eq. (29),

$$\left(\frac{K_{\rm B}T}{\rm keV}\right) = 22.445\mu f_T\left(\frac{\mathcal{M}}{10^{15}\mathcal{M}_\odot/{\rm h}}\right)\left(\frac{R_{\rm VIR}}{\rm Mpc/h}\right)^{-1} \times\left[1 + 3.8767\times10^{-4}\left(\frac{R_{\rm VIR}}{\rm Mpc/h}\right)^3\left(\frac{\mathcal{M}}{10^{15}\mathcal{M}_\odot/{\rm h}}\right)^{-1}\frac{\zeta_{\rm VIR}}{\bar{\rho}_0}\right], \tag{34}$$

where $f_T \propto 1/\beta$, would be the ratio of the actual temperature of the cluster compared to that obtained from our model. We determine $f_T$ from the extensive simulation results by Pen (1998). We take $f_T = 0.89 \pm 0.03$. This value represents a rough estimation of $f_T$; in fact we are comparing actual temperature to that derived by Pen, and the temperature from our model to that from the perfect isothermal sphere model (Eke et al. 1996). We should also say that the value of $f_T$ taken for us, coincides with the value proposed by Pen for the model by Bryan & Norman (1998).

Finally, defining $\Delta_{\rm c} = \frac{3\mathcal{M}c^2}{4\pi R_{\rm VIR}^3\bar{\rho}_{\rm m}}$, the mass-temperature relation can be expressed as

$$\left(\frac{\mathcal{M}}{10^{15}\mathcal{M}_\odot/{\rm h}}\right) = \left(\frac{K_{\rm B}T}{2.36\mu f_T\ {\rm keV}}\right)^{3/2}\left[\Omega_{\rm m0}(1+z_{\rm VIR})^3\Delta_{\rm c}\right]^{-1/2} \times\left[1 + \frac{\zeta_{\rm VIR}/\bar{\rho}_0}{3\Delta_{\rm c}\Omega_{\rm m0}(1+z_{\rm VIR})^3}\right]^{-3/2}. \tag{35}$$

### 4.4. Cumulative temperature function and $\sigma_8$

The temperature function, $\frac{{\rm d}n(T,z)}{{\rm d}T}$, is obtained from the number density of virialized objects per unit mass interval per comoving volume, $\frac{{\rm d}n(\mathcal{M},z)}{{\rm d}\mathcal{M}}$ (mass function), by $\frac{{\rm d}n(T,z)}{{\rm d}T} = \frac{{\rm d}n(\mathcal{M},z)}{{\rm d}\mathcal{M}}\frac{{\rm d}\mathcal{M}}{{\rm d}T}$. From the mass-temperature relation, calculated in the previous subsection, and from the Press-Schechter theory (Press & Schechter 1974),

$$\frac{{\rm d}n(\mathcal{M},z)}{{\rm d}\mathcal{M}} = -\sqrt{\frac{2}{\pi}}\frac{\bar{\rho}_m}{3\mathcal{M}}\frac{\delta_{\rm c}}{\sigma}\frac{{\rm d}\ln\sigma}{{\rm d}\ln R}\exp\left[-\frac{\delta_{\rm c}^2}{2\sigma^2}\right], \tag{36}$$

the integration of $\frac{{\rm d}n(T,\,z)}{{\rm d}T}$ on $T$ leads to the cumulative temperature function. In Eq. (36), $R = \left(\frac{3\mathcal{M}c^2}{4\pi\bar{\rho}_m}\right)^{1/3}$; $\sigma^2 = \int_0^\infty k^2\frac{P_0 kT_k^2}{2\pi^2}\left[\frac{3(\sin\ kR - kR\ \cos\ kR)}{(kR)^3}\right]^2{\rm d}k$ is the rms density fluctuations in tophat spheres on the comoving scale $R$; and, $\delta_{\rm c}$ is the linearly extrapolated overdensity that the fluctuation would have at the time of formation of the bound object. We have observed that the greater the $\Omega_{\rm m0}$ and $z_{\rm VIR}$ are, the greater the $\delta_{\rm c}$ is. With respect to $W$ and $\gamma$, we have seen that for the same $\gamma$, the greater the $|W|$ is, the greater the $\delta_{\rm c}(\gamma \le 1)$ and $\delta_{\rm c}(\gamma > 1, z > 0.1)$ are; and, for the same $|W|$, the greater the $\gamma$ is, the greater the $\delta_{\rm c}$ is. In any case the variations of $\delta_{\rm c}$ are small. As examples, for $\Omega_{\rm m0} = 0.27$, $W = -0.6$ and $\gamma = 0.5$, 1 and 2: $\delta_{\rm c} = 1.642$, 1.676 and 1.682 at $z = 0.01$; $\delta_{\rm c} = 1.651$, 1.686 and 1.688 at $z = 1$. For $\Omega_{\rm m0} = 0.27$ and $W = -1$: $\delta_{\rm c} = 1.679$ and 1.689 at $z = 0.01$ and 1. For $\Omega_{\rm m0} = 1$, $\delta_{\rm c} = 1.690$.

To derive $\sigma_8$, we have fit the theoretically predicted cumulative temperature function at $z = 0$ to that observed from the corrected Henry & Arnaud data (1991). Our results can be fitted by

$$\sigma_8 = 0.49\Omega_{\rm m0}^{0.04W - 0.22\Omega_{\rm m0} - 0.31}. \tag{37}$$

This fitting function is very accurate in the range of our study ($\Omega_{\rm m0} \in [0.23, 0.31]$, together with $\Omega_{\rm m0} = 1$); overall it is accurate within 0.5%. It should be noticed that, for the same $\Omega_{\rm m0}$ and $W$, the dependence of $\sigma_8$ on $\gamma$ is smaller than 0.1% in the range $[\gamma = 0.25, \gamma = 2.5]$; this result indicates again that, at $z = 0$, the magnitudes derived from our models show a small dependence on $\gamma$ (it is a consequence of the fact that $\rho_x(z \to 0)$ does not depend on $\gamma$ neither at zero nor at first order in $z$).

## 5. Numerical results and discussion

In this section, we present the results of this work with the aim of finding out if it is possible to discriminate dark energy models by comparing some magnitudes of collapsing regions (i.e. no virializad regions) of spherical clusters. We will dedicate special attention to shell velocities, from which, it is possible to derive observable redshifts. We have prefered to compare spherical cluster with the same $\sigma_{\rm los}$ due to the fact that velocity dispersions of clusters can be derived from observations (masses are only derived from observations when a ratio mass-luminosity is assumed). We will assume that $\sigma_{\rm los}$ is given by Eq. (29).

In Figs. 6–8, we present results for collapsing regions of several spherical clusters, at $z = 1$, 0.1 and 0.025, under different $\Omega_{\rm m0}, \gamma, W$ cosmologies. In these figures, the abscissa

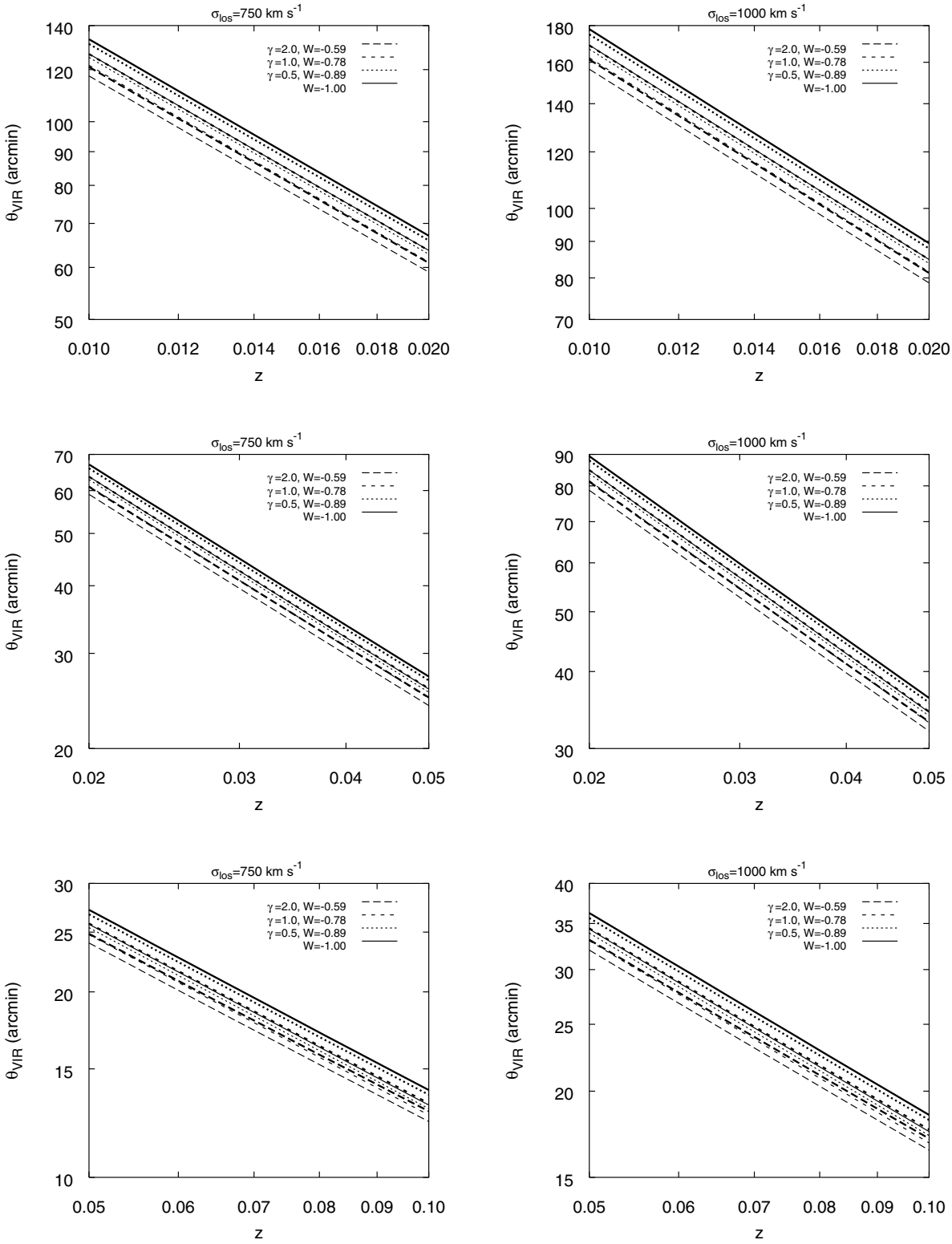


**Fig. 5.** Virial angular radii, $\theta_{\rm VIR}$, for $\sigma_{\rm los} = 750$ and 1000 km s$^{-1}$ spherical clusters, virialized at different redshifts, $z$. Several cosmological models have been considered (narrow lines correspond to $\Omega_{\rm m0} = 0.31$ cosmologies; wide lines to $\Omega_{\rm m0} = 0.23$).

axis represents the amounts $\theta = \arctan\left(r(1+z)\left[c\int_0^z \frac{{\rm d}z}{H(z)}\right]^{-1}\right)$, which can approximately be taken as the angular distance.

In Fig. 6, we deal with the $\Omega_{\rm m0} = 1$ model and with $\Omega_{\rm m0} = 0.31$ and 0.23 cosmological constant models. In this figure, modules of peculiar and proper velocities ($|v|$ and $|u|$) are shown for regions collapsing towards $\sigma_{\rm los} = 750$ and 1000 km s$^{-1}$ virialized spherical clusters (turn-around points are outstanding). From this figure, it can be seen that at $z = 0.1$ and $z = 0.025$, the greater the $\Omega_{\rm m0}$ is, the smaller the $|v|$ is.

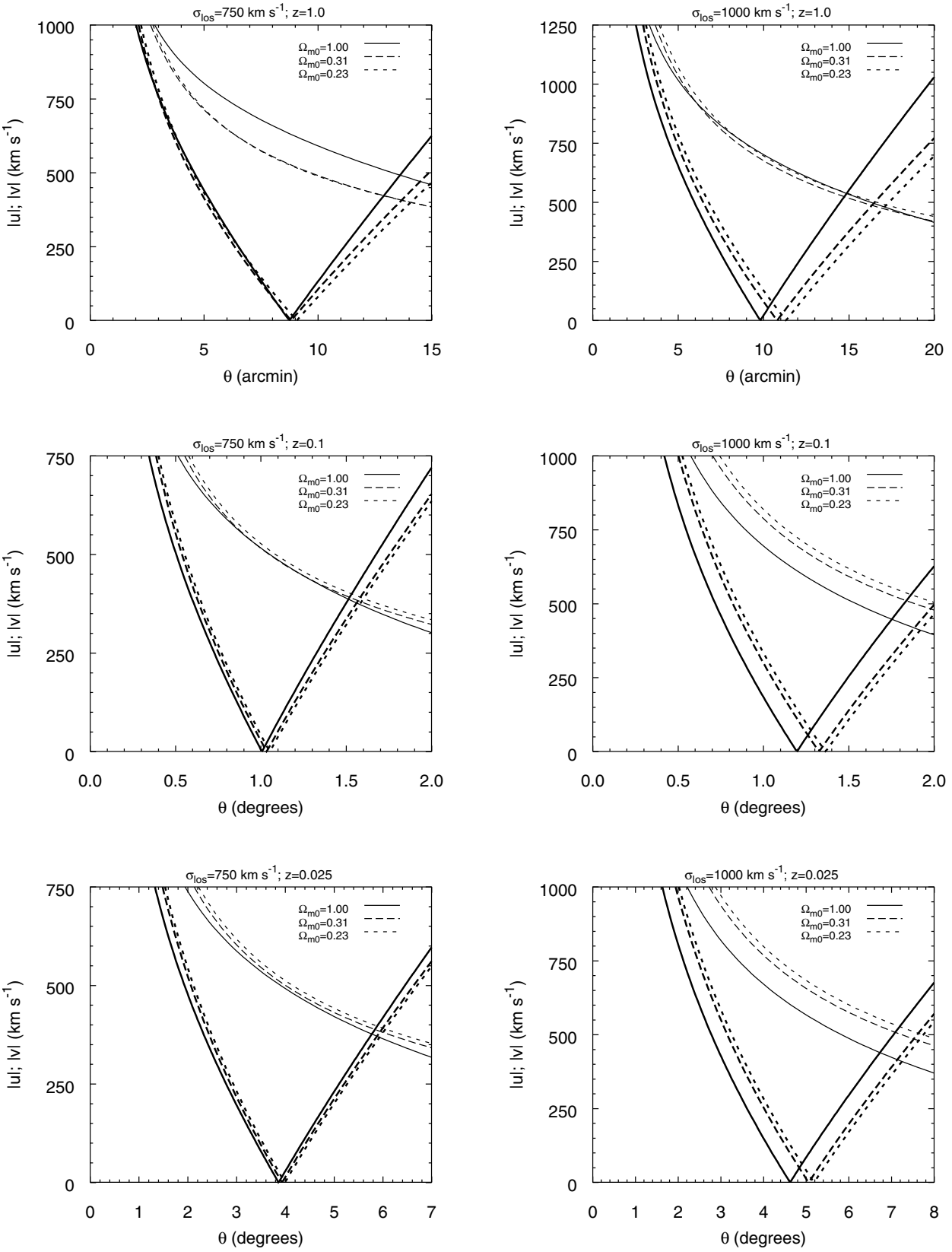


**Fig. 6.** Module of peculiar velocities $|v|$ (narrow lines) and module of proper velocities $|u|$ (wide lines) of shells collapsing towards the virialized region of $\sigma_{los} = 750$ km s$^{-1}$ and 1000 km s$^{-1}$ spherical clusters; several cosmological constant models have been considered.

To achieve a better appreciation of the differences among models, we present, in the left (right) panels of Figs. 7 and 8, the module of the difference between peculiar (proper) velocities of different $\Omega_{m0}, \gamma, W$ models and the $\Omega_{m0} = 1$ model,

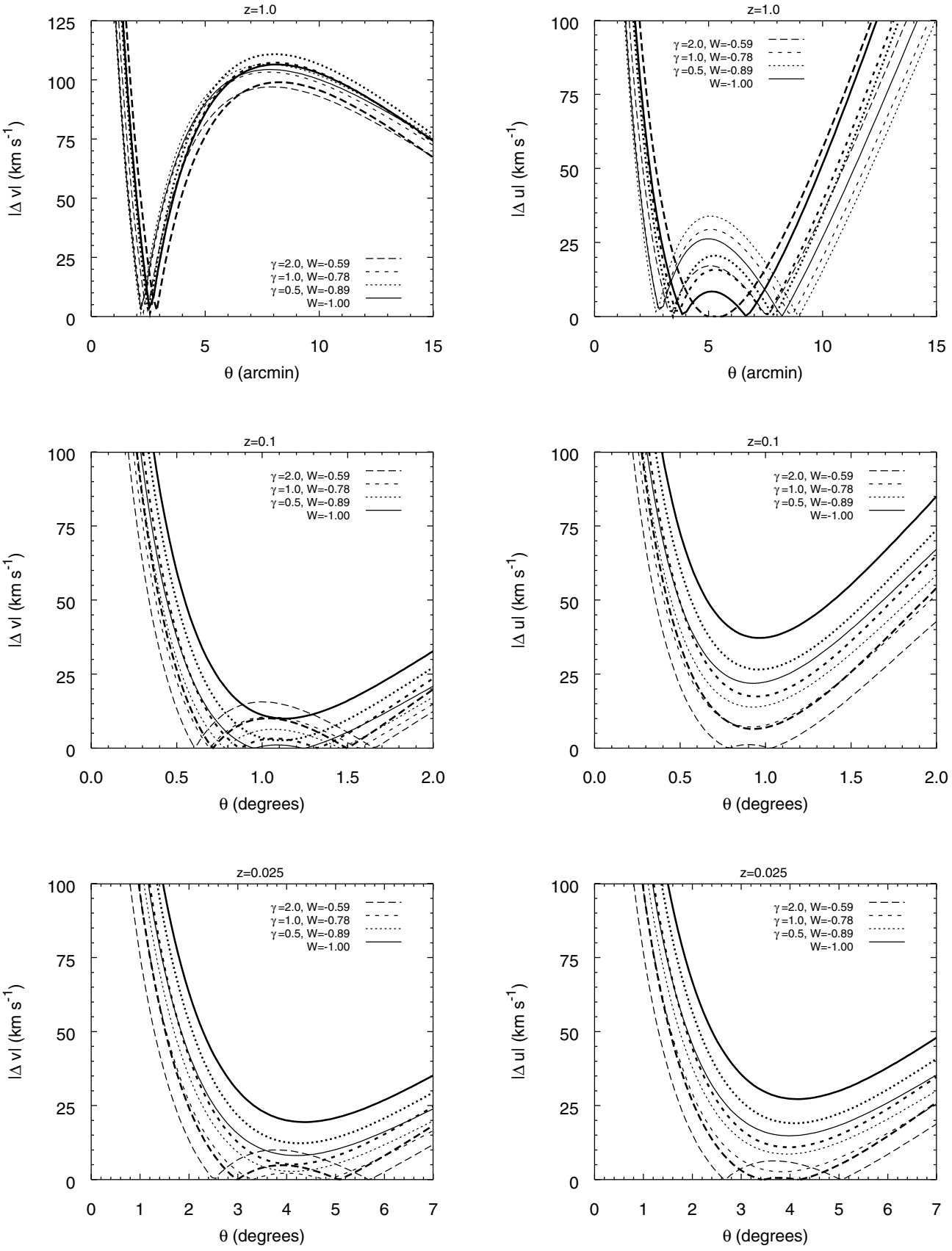


**Fig. 7.** *Left panels*: difference between peculiar velocities, $\Delta v = v_{\Omega_{m0},\gamma,W} - v_{\Omega_{m0}=1}$, of shells collapsing towards $\sigma_{los} = 750$ km s$^{-1}$ spherical clusters virialized at different redshifts. Several $\Omega_{m0}$, $\gamma$, $W$ cosmological background models have been taken into account; wide lines correspond to $\Omega_{m0} = 0.23$ and narrow lines to $\Omega_{m0} = 0.31$. *Right panels*: the same as in left panels for proper velocities, i.e., $\Delta u = u_{\Omega_{m0},\gamma,W} - u_{\Omega_{m0}=1}$.

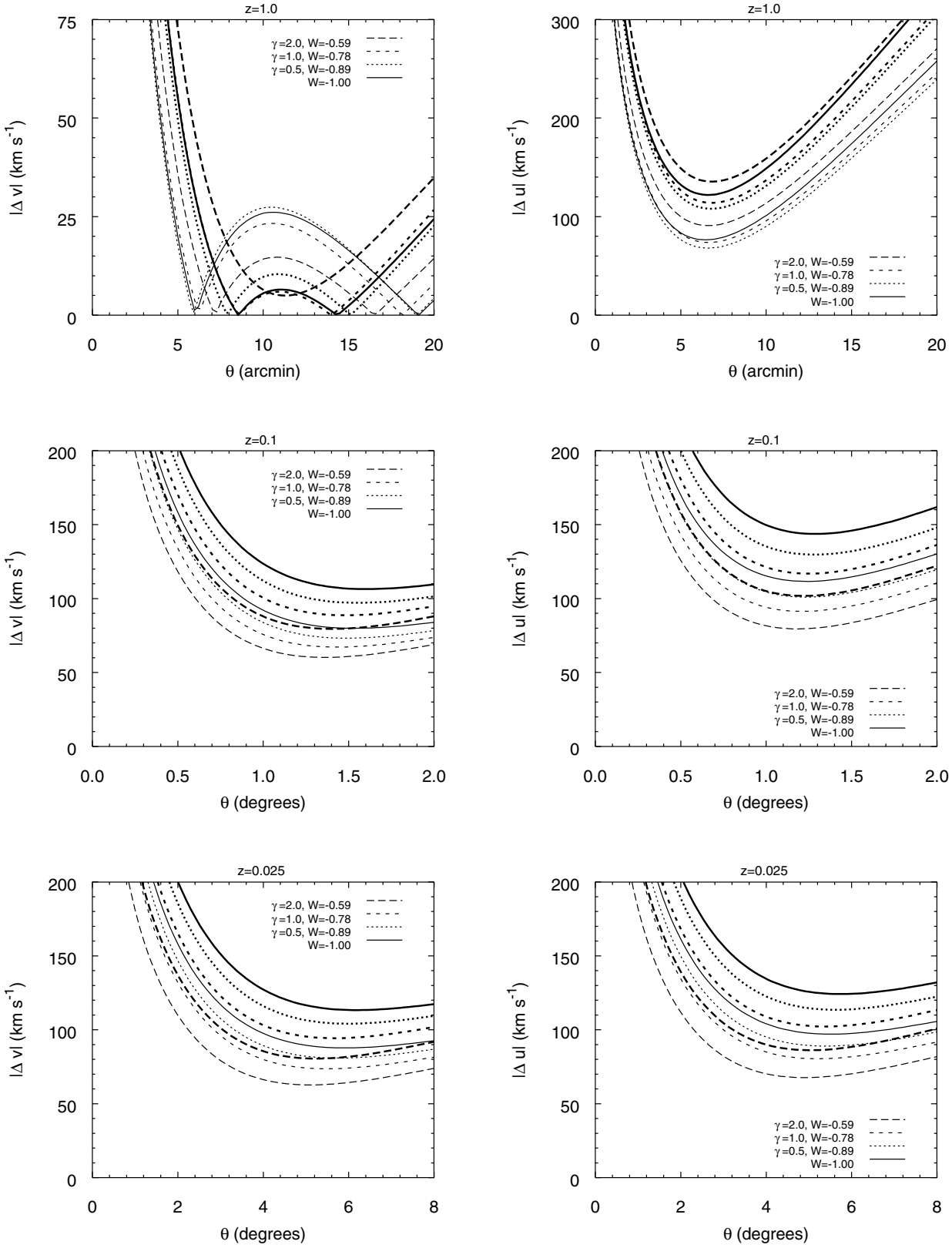


**Fig. 8.** The same as Fig. 7 for shells collapsing towards $\sigma_{los} = 1000$ km s$^{-1}$ spherical clusters virialized at different redshifts.

$|\Delta v|$ ($|\Delta u|$) (Fig. 6 can be used to derive $v$ and $u$). It can be seen in these figures that at the neighbourhood of the turn-around point of each model, there is a minimum or a maximum, $|\Delta v|_{TA}$ ($|\Delta u|_{TA}$). We will consider these values to make a comparison among models. Thus, we can say that, at $z = 1$, the $\gamma \geq 1$ models are closer than the $\gamma < 1$ ones to cosmological constant models; this is a consequence of the behaviour of the dark energy densities of $\gamma < 1$ models at $z \gg 1$ (they behave as matter does). However, at $z = 0.1$ and 0.025, the $\gamma < 1$ models are the closest ones to cosmological constant models. This means

that at $z < 1$, it begins to affect the other asymptotic behaviours of our dark energy densities ($\gamma > 1$ models tend to behave as matter does and $\gamma < 1$ models as cosmological constant does). We note that the larger the $\sigma_{los}$ is, the greater $|\Delta v|_{TA}$ and $|\Delta u|_{TA}$ are: they are smaller than 45 km s$^{-1}$ for $\sigma_{los} = 750$ km s$^{-1}$ (except for peculiar velocities at $z = 1$), and take values from 60 up to 150 km s$^{-1}$ for $\sigma_{los} = 1000$ km s$^{-1}$ (we have also seen that for $\sigma_{los} = 1500$ km s$^{-1}$ and for some of the studied models they reach up to 400 km s$^{-1}$). As a consequence, the differences between peculiar (proper) velocities of the two considered cosmological constant models grow with $\sigma_{los}$; in fact, for $\sigma_{los} = 750$ km s$^{-1}$, they are about 15−20 km s$^{-1}$ and 30−35 km s$^{-1}$ for $\sigma_{los} = 1000$ km s$^{-1}$ (for $\sigma_{los} = 1500$ km s$^{-1}$, they are greater than 60 km s$^{-1}$, reaching 120 km s$^{-1}$ at $z = 1$). According to our results, the two studied cosmological constant models could be discriminated for $\sigma_{los} \geq 1000$ km s$^{-1}$. Finally, we can say that $|\Delta v|$ and $|\Delta u|$ do not show a great difference from $z = 0.1$; so, it would be more useful to deal with small redshifts in order to compare with observations.

It should also be said that all the above differences increase as $\Omega_{m0}$ is taken smaller; as examples, for $\Omega_{m0} = 0.1$ ($\Omega_{m0} = 0.05$) and $\sigma_{los} = 1000$ km s$^{-1}$, $|\Delta v|_{TA}$ and $|\Delta u|_{TA}$ take values greater than 150 km s$^{-1}$ (200 km s$^{-1}$), and some models even reach values greater than 300 km s$^{-1}$ (400 km s$^{-1}$) ($|\Delta u|_{TA}$ for the cosmological constant model at $z = 1$).

As redshifts of galaxies in clusters, and angular separations among cluster centres and galaxy positions are observables, we have thought that it would be very interesting to have a look to the effects of different cosmolocial backgrounds on caustics. When dealing with clusters of galaxies, the position of the cluster centre at redshift $z$ is given by $R(z) = \frac{R_0}{1+z}$, with $R_0 = c\int_0^z \frac{dz'}{H(z')}$. According to our study, if the localization of a galaxy in the cluster is $r(z)$, then, the galaxy is in a shell whose radius and peculiar velocity are given by Eqs. (13) and (22), respectively. In the redshift space, the position of the galaxy is fixed by its redshift $z_g$ and the angle $\phi$ from the direction of the cluster centre. For $z \ll 1$ it is easy to show that

$$cz_g = H_0 R_0 \cos\phi \pm (H_0 r - |\, v\,|)\sqrt{1 - \left(\frac{R_0}{r}\right)^2 \sin^2\phi}. \qquad (38)$$

The caustics are, then, found in the redshift space at the points $(z_{g_c}, \phi_c)$ where the density of galaxies is infinity, i.e., where (see, for example, Regös & Geller 1989),

$$\cos^2\phi_c = \frac{1 - \frac{r}{u}\frac{du}{dr}\left[1 - \left(\frac{r}{R}\right)^2\right]}{1 - \frac{r}{u}\frac{du}{dr}}. \qquad (39)$$

Because of the observability of caustics is greater at small redshifts, and as the diference between peculiar (proper) velocities of $\Omega_{m0} = 1$ and $\Omega_{m0}, \gamma, W$ models is similar from $z = 0.1$, we have chosen $z = 0.025$ spherical clusters to study their caustics.

In order to see the dependence on $\sigma_{los}$, we have studied spherical clusters with three different velocity dispersions of the virialized structures: $\sigma_{los} = 750, 1000, 1500$ km s$^{-1}$. In the right panels of Fig. 9, we present caustics, $cz_c(\phi)$, for the $\Omega_{m0} = 1$ model and for the cosmological constant models $\Omega_{m0} = 0.23$ and $\Omega_{m0} = 0.31$. Again, to achieve a better appreciation of the differences among models, we show, in the lefts panels of Fig. 9, the diferences between upper branches of caustics of several $\Omega_{m0}, \gamma, W$ models and the $\Omega_{m0} = 1$ model, $\Delta cz_c(\phi)$.

We notice that $\Delta cz_c(\phi)$ grows as $\sigma_{los}$ is taken greater. We also observe that models, whose behaviour results similar or equal to that of the cosmological constant model (i.e., $W = -1$ and $\gamma < 1$ models), show a value of $\Delta cz_c$ greater than those of the rest of models ($\gamma \geq 1$). According with our results, $\Delta cz_c$ could reach values greater than the observational errors of meassurement. This would mean that, from observations of caustics of $z = 0.025$ spherical clusters, it could be possible distinguish $\Omega_{m0} = 0.23$ ... 0.31 dark energy models from the $\Omega_{m0} = 1$ model; however, it would be more difficult to discriminate among dark energy models. We think that only if cosmological constant models were the only valid models, the determination of $\Omega_{m0}$ could be possible from caustic observations of $\sigma_{los} \geq 1000$ km s$^{-1}$ spherical clusters (caustics of $\Omega_{m0} = 0.23$ and $\Omega_{m0} = 0.31$ differ in more than 30 km s$^{-1}$; if $\Omega_{m0}$ is taken smaller, such differences increase (they reach up to 85 km s$^{-1}$ and 120 km s$^{-1}$ for $\Omega_{m0} = 1$ and 0.05, respectivelly).

## 6. Conclusions

1. The aim of this work has been to find out if it is possible to discriminate dark energy models from shell velocities derived from the study of the spherical collapse of matter perturbations.
2. Instead of doing a hard work studying a great number of models, for the sake of simplicity, we have chosen a simple dark energy model ($\omega_x = \frac{p_x}{\rho_x} = W\left(\frac{\rho_x}{\rho_{x0}}\right)^{\gamma-1}$). This model show a great number of behaviours of the kind $\omega$-slowly and strongly varying and $\omega$-constant, with just two parameters. To estimate model parameters we have use WMAP and other data.
3. From proper and peculiar velocities of collapsing shells, we have seen that, at $z = 1$, the $\gamma \geq 1$ models are more similar than the $\gamma < 1$ ones to cosmological constant models. However, at $z \leq 0.1$, $\gamma < 1$ models are the nearest to a cosmological constant. The reason is found in the asymptotic behaviour of our dark energy densities.
4. We have noticed, from shell velocities, that the difference between our dark energy models and the $\Omega_{m0} = 1$ model grows as the line-of-sight velocity dispersion, $\sigma_{los}$, of the virialized structure is greater. We can say that our models are clearly differenced from $\Omega_{m0} = 1$; in fact, for $\sigma_{los} \geq 1000$ km s$^{-1}$ they show modules of proper and peculiar velocities which are 60 km s$^{-1}$ greater than those of the $\Omega_{m0} = 1$ model (more than 100 km s$^{-1}$ for the cosmological constant models $\Omega_{m0} = 0.31$ and $\Omega_{m0} = 0.23$).
5. According to shell velocities, the differences among our dark energy models are not so large. Moreover, similar velocity profiles could be reproduced with different $\Omega_{m0}, \gamma, W$ models. In any case, for $\sigma_{los} \geq 1000$ km s$^{-1}$, proper and peculiar velocities of the two studied cosmological constant models differ in more than 30 km s$^{-1}$.
6. As our results do not show a great difference from $z = 0.1$, it seems to be more useful to deal with nearby clusters to compare with observations.

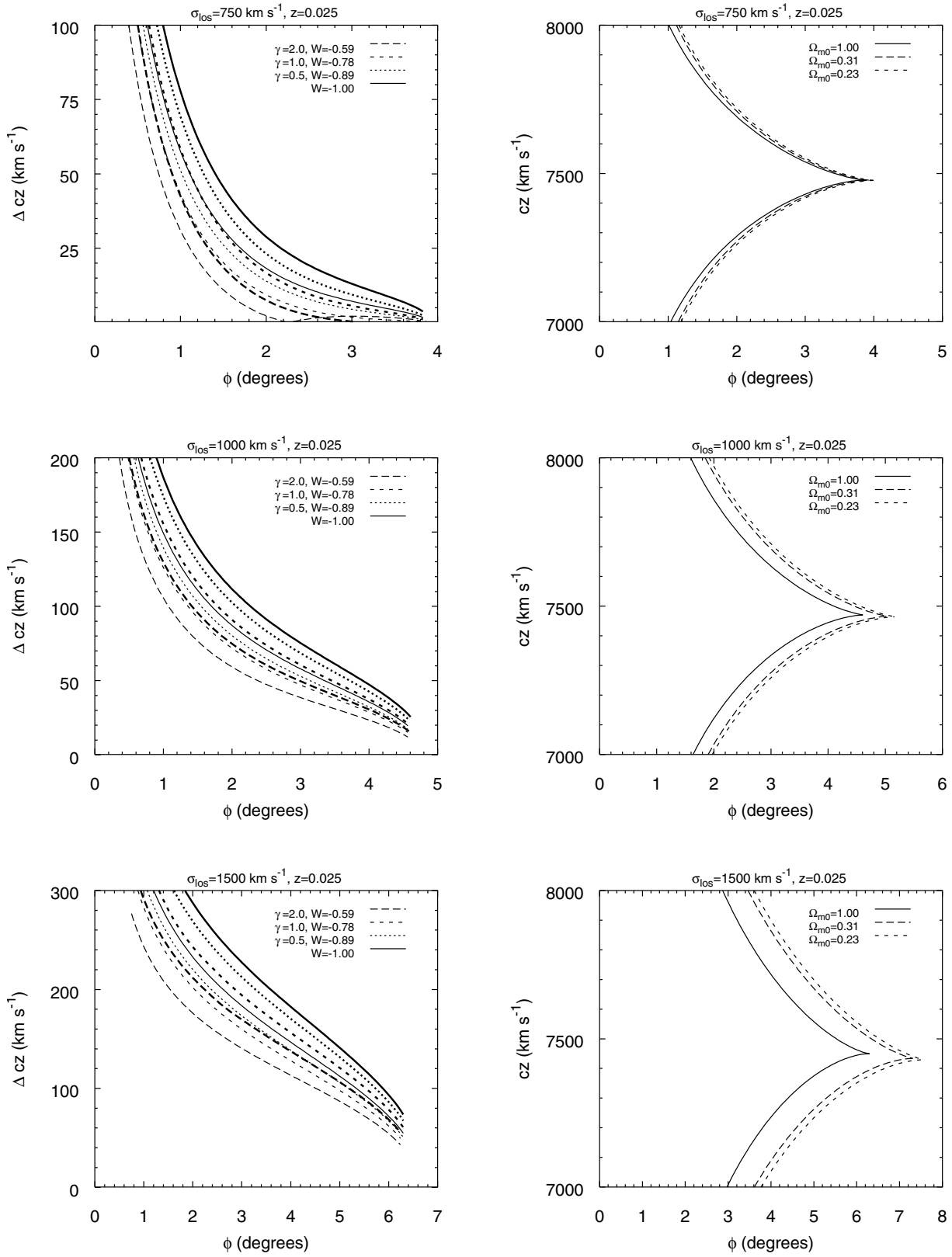


**Fig. 9.** Caustics of several $z = 0.025$ spherical clusters. *Left panels*: $\Delta cz_c(\phi) = cz_{c_{\Omega_{m0},\gamma,W}}(\phi) - cz_{c_{\Omega_{m0}=1}}(\phi)$ for the upper branch of spherical cluster caustics under several cosmological backgrounds; wide lines correspond to $\Omega_{m0} = 0.23$, while narrow ones to $\Omega_{m0} = 0.31$. *Right panels*: caustics $cz_c(\phi)$ for some cosmological constant models.

7. Our study of caustics in theoretical $z = 0.025$ spherical clusters confirms the above conclusions. Thus, we think that from observations of caustics of nearby spherical clusters, it would be possible to discriminate cosmological

constant models from the $\Omega_{m0} = 1$ model, being more difficult to distinguish among dark energy models.

8. In the next future a number of surveys (2dF, 6dF, SDSS, SKA, ...) will provide us information about the large scale structure of the universe. They will give us information about the redshift of millions of nearby and distant objects which will be useful for the restrictions of the cosmological parameters. In particular, they will give us information of distant clusters and they will be useful for discriminating about the existence or not of the cosmological constant as was pointed in previous sections of the present work.

*Acknowledgements.* This work was supported by the Spanish MCYT project AYA 2003-00128. JALA was partially financed by the project AYA2001-3939-C03 of the Spanish Programa Nacional de Astronomia y Astrofisica of the MCYT.

## References

Aguerri, J. A. L., & Membrado, M. 1999, MNRAS, 302, 625
Bardeen, J. M., Bond, J. R., Raise, N., & Szalay, A. S. 1986, ApJ, 304, 15 (BBKS)
Battye, R. A., & Weller, J. 2003, Phys. Rev. D, 68, 083506
Barrow, J. 1988, Nucl. Phys. B, 310, 743
Bertschinger, E. 1990, Proc. of the Moriond Conf.
Binney, J., & Tremaine, S. 1994, Galactic dynamics (Princeton: Princeton Univ. Press)
Bloomfield-Torres, L. F., & Waga, I. 1996, MNRAS, 279, 712
Bronstein, M. 1933, Phys. Zeit. Sowjet Union, 3, 73
Bryan, G. L., & Norman, M. L. 1998, ApJ, 495, 80
Cadwell, R. R., Dave, R., & Steinhardt, P. J. 1998, Phys. Rev. Lett., 80, 1582
Chaboyer, B., Denmarque, P., Kernan, P. L., & Krauss, L. M. 1995, Science, 271, 957
Coble, et al. 1996, Phys. Rev. D, 55, 1851
Cole, S., & Lacey, C. 1996, MNRAS, 281, 716
Dekel, A., Bertschinger, E., & Faber, S. M. 1990, ApJ, 364, 349
Efstathiou, G., Bond, J. R., & White, S. D. M. 1992, MNRAS, 258, 1p
Efstathiou, G., Bridle, S. L., Lasenby, A. N., Hobson, M. P., Ellis, R. S., et al. 1998 [arXiv:astro-ph/9812226]
Eke, V. R., Cole, S., & Frenk, C. S. 1996, MNRAS, 282, 263
Freese, K., Adams, F. C., Frieman, J. A., & Mottola, E. 1987, Nucl. Phys. B, 287, 797
Frieman, J. A., Hill, C. T., Stebbins, A., & Waga, I. 1995, Phys. Rev. Lett., 75, 2077
Goobar, A., Mörtsell, E., & Amanullah, R. 2002, A&A, 392, 757
Groth, E. J., & Peebles, P. J. E. 1975, A&A, 41, 143
Gunn, J. E., & Gott, J. R. 1972, ApJ, 176, 1
Hawkins, E., Maddox, S., Cole, S., et al. 2003, MNRAS, 346, 78
Henry, J. P., & Arnaud, K. A. 1991, ApJ, 372, 410
Huey, G., Wang, L., Dave, R., Caldwell, R. R., & Steinhardt, P. J. 1999, Phys. Rev. D, 59, 063005
Kaiser, N., Efstathiou, G., Saunders, W., et al. 1991, MNRAS, 252, 1
Lahav, O., Lilje, P. B., Primack, J. R., & Rees, M. J. 1991, MNRAS, 251, 128
Lahav, O., Bridle, S. L., Percival, W. J., et al. 2002, MNRAS, 333, 961
Lokas, E. L. 2001, Acta Phys. Pol. B, 32, 3643
Lidsey, J. 1994, MNRAS, 266, 489
Lynden-Bell, D., Lahav, O., & Burstein, D. 1989, MNRAS, 241, 325
Maor, I., & Brustein, R. 2003, Phys. Rev. D, 67, 103508
Mészáros, P. 1974, A&A, 37, 225
Membrado, M. 2004, in preparation
Ozer, M., & Taha, M. O. 1987, Nucl. Phys. B, 287, 776
Peebles, P. J. E. 1980, The large scale structure of the Universe (Princeton: Princeton Univ. Press)
Peebles, P. J. E. 1984, ApJ, 284, 439
Pen, U.-L. 1998, ApJ, 498, 60
Perlmutter, S., Aldering, G., Deustua, S., et al. 1997, BAAS, 29, 1351 [arXiv:astro-ph/9812473]
Perlmutter, S., Aldering, G., Goldhaber, G., et al. 1999, ApJ, 517, 565
Press, W. H., & Schechter, P. 1974, ApJ, 187, 425
Ratra, B., & Peebles, P. J. E. 1988, Phys. Rev. D, 37, 3406
Regös, E., & Geller, M. J. 1989, AJ, 98, 755
Schmidt, B., Suntzeff, N. B., Phillips, M. M., et al. 1998, ApJ, 507, 46
Spergel, D., & Pen, U.-L. 1997, ApJ, 441, L67
Spergel, D. N., Verde, L., Peiris, H. V., et al. 2003, ApJS, 148, 175
Steinhardt, P. J. 1996, Nature, 382, 768
Strauss, M. 1989, Ph.D. Thesis, University of California, Berkeley
Sugiyama, N. 1995, ApJS, 100, 281
Turner, M. S., & White, M. 1997, Phys. Rev. D, 56, 4439
Vilenkin, A. 1984, Phys. Rev. Lett, 53, 1016
Wang, L., & Steinhardt, P. J. 1998, ApJ, 508, 483
Weinberg, S. 1987, Phys. Rev. Lett., 59, 2607
Wetterich, C. 1988, Nucl. Phys. B, 302, 668
Wetterich, C. 1995, A&A, 301, 321
Yahil, A. 1985, The Virgo Cluster of galaxies, p. 395, ed. O. G. Richter, & B. Binggeli, ESO, Garching
Yahil, A. 1990, Proc. of the Moriond Conf.
Yahil, A., Strauss, M. A., Davis, M., & Huchra, J. P. 1991, ApJ, 372, 380
Zlatev, I., Wang, L., & Steinhardt, P. J. 1999, Phys. Rev. Lett, 82, 896